Chapter 1
Introduction – Measurement Techniques and Applications

Bharat Bhushan

In this introductory chapter, the definition and history of tribology and their industrial significance and origins and significance of an emerging field of micro/nanotribology are described. Next, various measurement techniques used in micro/nanotribological and micro/nanomechanical studies are described. The interest in micro/nanotribology field grew from magnetic storage devices and latter the applicability to emerging field micro/nanoelectromechanical systems (MEMS/NEMS) became clear. A few examples of magnetic storage devices and MEMS/NEMS are presented where micro/nanotribological and micro/nanomechanical tools and techniques are essential for interfacial studies. Finally, reasons why micro/nanotribological and micro/nanomechanical studies are important in magnetic storage devices and MEMS/NEMS are presented. In the last section, organization of the book is presented.

1.1 Definition and History of Tribology

The word tribology was first reported in a landmark report by Jost [1]. The word is derived from the Greek word tribos meaning rubbing, so the literal translation would be "the science of rubbing". Its popular English language equivalent is friction and wear or lubrication science, alternatively used. The latter term is hardly all-inclusive. Dictionaries define tribology as the science and technology of interacting surfaces in relative motion and of related subjects and practices. Tribology is the art of applying operational analysis to problems of great economic significance, namely, reliability, maintenance, and wear of technical equipment, ranging from spacecraft to household appliances. Surface interactions in a tribological interface are highly complex, and their understanding requires knowledge of various disciplines including physics, chemistry, applied mathematics, solid mechanics, fluid mechanics, thermodynamics, heat transfer, materials science, rheology, lubrication, machine design, performance and reliability.

It is only the name tribology that is relatively new, because interest in the constituent parts of tribology is older than recorded history [2]. It is known that

B. Bhushan (ed.), *Nanotribology and Nanomechanics*,
DOI 10.1007/978-3-642-15283-2_1,

drills made during the Paleolithic period for drilling holes or producing fire were fitted with bearings made from antlers or bones, and potters' wheels or stones for grinding cereals, etc., clearly had a requirement for some form of bearings [3]. A ball thrust bearing dated about AD 40 was found in Lake Nimi near Rome.

Records show the use of wheels from 3500 BC, which illustrates our ancestors' concern with reducing friction in translationary motion. The transportation of large stone building blocks and monuments required the know-how of frictional devices and lubricants, such as water-lubricated sleds. Figure 1.1 illustrates the use of a sledge to transport a heavy statue by egyptians circa 1880 BC [4]. In this transportation, 172 slaves are being used to drag a large statue weighing about 600 kN along a wooden track. One man, standing on the sledge supporting the statue, is seen pouring a liquid (most likely water) into the path of motion; perhaps he was one of the earliest lubrication engineers. (Dowson [2] has estimated that each man exerted a pull of about 800 N. On this basis, the total effort, which must at least equal the friction force, becomes 172×800 N. Thus, the coefficient of friction is about 0.23.) A tomb in Egypt that was dated several thousand years BC provides the evidence of use of lubricants. A chariot in this tomb still contained some of the original animal-fat lubricant in its wheel bearings.

During and after the glory of the Roman empire, military engineers rose to prominence by devising both war machinery and methods of fortification, using tribological principles. It was the renaissance engineer-artist Leonardo da Vinci (1452–1519), celebrated in his days for his genius in military construction as well as for his painting and sculpture, who first postulated a scientific approach to friction. Da Vinci deduced the rules governing the motion of a rectangular block sliding over a flat surface. He introduced for the first time, the concept of coefficient of friction as the ratio of the friction force to normal load. His work had no historical influence, however, because his notebooks remained unpublished for hundreds of years. In 1699, the French physicist Guillaume Amontons rediscovered the rules of friction after he studied dry sliding between two flat surfaces [5]. First, the friction force that resists sliding at an interface is directly proportional to the normal load.

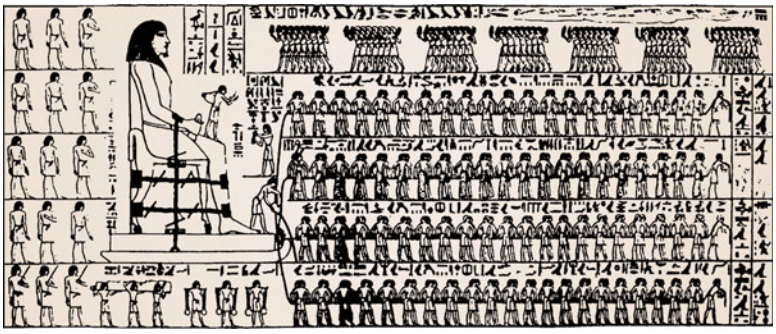

Fig. 1.1 Egyptians using lubricant to aid movement of colossus, El-Bersheh, circa 1800 BC

Second, the amount of friction force does not depend on the apparent area of contact. These observations were verified by French physicist Charles-Augustin Coulomb (better known for his work on electrostatics [6]). He added a third rule that the friction force is independent of velocity once motion starts. He also made a clear distinction between static friction and kinetic friction.

Many other developments occurred during the 1500s, particularly in the use of improved bearing materials. In 1684, Robert Hooke suggested the combination of steel shafts and bell-metal bushes as preferable to wood shod with iron for wheel bearings. Further developments were associated with the growth of industrialization in the latter part of the eighteenth century. Early developments in the petroleum industry started in Scotland, Canada, and the United States in the 1850s [2–7].

Though essential laws of viscous flow were postulated by Sir Isaac Newton in 1668; scientific understanding of lubricated bearing operations did not occur until the end of the nineteenth century. Indeed, the beginning of our understanding of the principle of hydrodynamic lubrication was made possible by the experimental studies of Tower [8] and the theoretical interpretations of Reynolds [9] and related work by Petroff [10]. Since then developments in hydrodynamic bearing theory and practice were extremely rapid in meeting the demand for reliable bearings in new machinery.

Wear is a much younger subject than friction and bearing development, and it was initiated on a largely empirical basis. Scientific studies of wear developed little until the mid-twentieth century. Holm made one of the earliest substantial contributions to the study of wear [11].

The industrial revolution (1750–1850 A.D.) is recognized as a period of rapid and impressive development of the machinery of production. The use of steam power and the subsequent development of the railways in the 1830s led to promotion of manufacturing skills. Since the beginning of the twentieth century, from enormous industrial growth leading to demand for better tribology, knowledge in all areas of tribology has expanded tremendously [11–17].

1.2 Industrial Significance of Tribology

Tribology is crucial to modern machinery which uses sliding and rolling surfaces. Examples of productive friction are brakes, clutches, driving wheels on trains and automobiles, bolts, and nuts. Examples of productive wear are writing with a pencil, machining, polishing, and shaving. Examples of unproductive friction and wear are internal combustion and aircraft engines, gears, cams, bearings, and seals.

According to some estimates, losses resulting from ignorance of tribology amount in the United States to about 4% of its gross national product (or about $ 200 billion dollars per year in 1966), and approximately one-third of the world's energy resources in present use appear as friction in one form or another. Thus, the importance of friction reduction and wear control cannot be overemphasized for economic reasons and long-term reliability. According to Jost [1, 18], savings of about 1% of gross national product of an industrialized nation can be realized by

research and better tribological practices. According to recent studies, expected savings are expected to be on the order of 50 times the research costs. The savings are both substantial and significant, and these savings can be obtained without the deployment of large capital investment.

The purpose of research in tribology is understandably the minimization and elimination of losses resulting from friction and wear at all levels of technology where the rubbing of surfaces is involved. Research in tribology leads to greater plant efficiency, better performance, fewer breakdowns, and significant savings.

Tribology is not only important to industry, it also affects day-to-day life. For example, writing is a tribological process. Writing is accomplished by a controlled transfer of lead (pencil) or ink (pen) to the paper. During writing with a pencil there should be good adhesion between the lead and paper so that a small quantity of lead transfers to the paper and the lead should have adequate toughness/hardness so that it does not fracture/break. Objective during shaving is to remove hair from the body as efficiently as possible with minimum discomfort to the skin. Shaving cream is used as a lubricant to minimize friction between a razor and the skin. Friction is helpful during walking and driving. Without adequate friction, we would slip and a car would skid! Tribology is also important in sports. For example, a low friction between the skis and the ice is desirable during skiing.

1.3 Origins and Significance of Micro/Nanotribology

At most interfaces of technological relevance, contact occurs at numerous asperities. Consequently, the importance of investigating a single asperity contact in studies of the fundamental tribological and mechanical properties of surfaces has been long recognized. The recent emergence and proliferation of proximal probes, in particular tip-based microscopies (e.g., the scanning tunneling microscope and the atomic force microscope) and of computational techniques for simulating tip-surface interactions and interfacial properties, has allowed systematic investigations of interfacial problems with high resolution as well as ways and means for modifying and manipulating nanoscale structures. These advances have led to the development of the new field of microtribology, nanotribology, molecular tribology, or atomic-scale tribology [15, 16, 19–22]. This field is concerned with experimental and theoretical investigations of processes ranging from atomic and molecular scales to microscales, occurring during adhesion, friction, wear, and thin-film lubrication at sliding surfaces.

The differences between the conventional or macrotribology and micro/nanotribology are contrasted in Fig. 1.2. In macrotribology, tests are conducted on components with relatively large mass under heavily loaded conditions. In these tests, wear is inevitable and the bulk properties of mating components dominate the tribological performance. In micro/nanotribology, measurements are made on components, at least one of the mating components, with relatively small mass

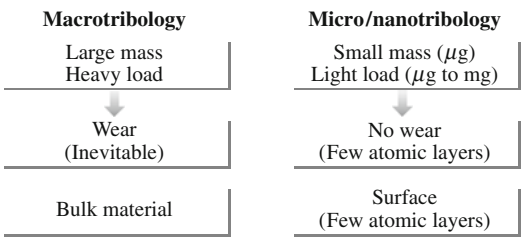

Fig. 1.2 Comparisons between macrotribology and micro/nanotribology

under lightly loaded conditions. In this situation, negligible wear occurs and the surface properties dominate the tribological performance.

The micro/nanotribological studies are needed to develop fundamental understanding of interfacial phenomena on a small scale and to study interfacial phenomena involving ultrathin films (as low as 1–2 nm) and in micro/nanostructures, both used in magnetic storage systems, micro/nanoelectromechanical systems (MEMS/NEMS) and other industrial applications. The components used in micro- and nanostructures are very light (on the order of few micrograms) and operate under very light loads (smaller than 1 μg to a few milligrams). As a result, friction and wear (on a nanoscale) of lightly loaded micro/nanocomponents are highly dependent on the surface interactions (few atomic layers). These structures are generally lubricated with molecularly thin films. Micro/nanotribological techniques are ideal to study the friction and wear processes of ultrathin films and micro/nanostructures. Although micro/nanotribological studies are critical to study ultrathin films and micro/nanostructures, these studies are also valuable in fundamental understanding of interfacial phenomena in macrostructures to provide a bridge between science and engineering.

The probe-based microscopes (scanning tunneling microscope, the atomic force and friction force microscopes) and the surface force apparatus are widely used for micro/nanotribological studies [16, 19–23]. To give a historical perspective of the field, the scanning tunneling microscope (STM) developed by Binnig and Rohrer and their colleagues in 1981 at the IBM Zurich Research Laboratory, Forschungslabor, is the first instrument capable of directly obtaining three-dimensional (3-D) images of solid surfaces with atomic resolution [24]. STMs can only be used to study surfaces which are electrically conductive to some degree. Based on their design of STM, in 1985, Binnig et al. [25, 26] developed an atomic force microscope (AFM) to measure ultrasmall forces (less than 1 μN) present between the AFM tip surface and the sample surface. AFMs can be used for measurement of all engineering surfaces which may be either electrically conducting or insulating. AFM has become a popular surface profiler for topographic measurements on micro – to nanoscale. AFMs modified to measure both normal and friction forces, generally called friction force microscopes (FFMs) or lateral force microscopes (LFMs), are used to measure friction on micro- and nanoscales. AFMs are also used for studies of adhesion, scratching, wear, lubrication, surface temperatures,

and for measurements of elastic/plastic mechanical properties (such as indentation hardness and modulus of elasticity) [14, 16, 19, 21].

Surface force apparatuses (SFAs), first developed in 1969, are used to study both static and dynamic properties of the molecularly thin liquid films sandwiched between two molecularly smooth surfaces [16, 20–22, 27]. However, the liquid under study has to be confined between molecularly-smooth optically-transparent or sometimes opaque surfaces with radii of curvature on the order of 1 mm (leading to poorer lateral resolution as compared to AFMs). Only AFMs/FFMs can be used to study engineering surfaces in the dry and wet conditions with atomic resolution.

Meanwhile, significant progress in understanding the fundamental nature of bonding and interactions in materials, combined with advances in computer-based modeling and simulation methods, have allowed theoretical studies of complex interfacial phenomena with high resolution in space and time [16, 20–22]. Such simulations provide insights into atomic-scale energetics, structure, dynamics, thermodynamics, transport and rheological aspects of tribological processes. Furthermore, these theoretical approaches guide the interpretation of experimental data and the design of new experiments, and enable the prediction of new phenomena based on atomistic principles.

1.4 Measurement Techniques

1.4.1 Scanning Probe Microscopy

Family of instruments based on STMs and AFMs, called Scanning Probe Microscopes (SPMs), have been developed for various applications of scientific and industrial interest. These include – STM, AFM, FFM (or LFM), scanning electrostatic force microscopy (SEFM), scanning force acoustic microscopy (SFAM) (or atomic force acoustic microscopy, AFAM), scanning magnetic microscopy (SMM) (or magnetic force microscopy, MFM), scanning near field optical microscopy (SNOM), scanning thermal microscopy (SThM) scanning electrochemical microscopy (SEcM), scanning Kelvin Probe microscopy (SKPM), scanning chemical potential microscopy (SCPM), scanning ion conductance microscopy (SICM), and scanning capacitance microscopy (SCM). Family of instruments which measure forces (e.g. AFM, FFM, SEFM, SFAM, and SSM) are also referred to as scanning force microscopies (SFM). Although these instruments offer atomic resolution and are ideal for basic research, yet these are used for cutting edge industrial applications which do not require atomic resolution.

STMs, AFMs and their modifications can be used at extreme magnifications ranging from $10^3\times$ to $10^9\times$ in x-, y-, and z-directions for imaging macro to atomic dimensions with high-resolution information and for spectroscopy. These instruments can be used in any environment such as ambient air, various gases, liquid, vacuum, low temperatures, and high temperatures. Imaging in liquid allows the

study of live biological samples and it also eliminates water capillary forces present in ambient air present at the tip–sample interface. Low temperature imaging is useful for the study of biological and organic materials and the study of low-temperature phenomena such as superconductivity or charge-density waves. Low-temperature operation is also advantageous for high-sensitivity force mapping due to the reduction in thermal vibration. These instruments also have been used to image liquids such as liquid crystals and lubricant molecules on graphite surfaces. While the pure imaging capabilities of SPM techniques dominated the application of these methods at their early development stages, the physics and chemistry of probe–sample interactions and the quantitative analyses of tribological, electronic, magnetic, biological, and chemical surfaces are commonly carried out. Nanoscale science and technology are strongly driven by SPMs which allow investigation and manipulation of surfaces down to the atomic scale. With growing understanding of the underlying interaction mechanisms, SPMs have found applications in many fields outside basic research fields. In addition, various derivatives of all these methods have been developed for special applications, some of them targeting far beyond microscopy.

A detailed overview of scanning probe microscopy – principle of operation, instrumentation, and probes is presented in a later chapter (also see [16, 20–23]). Here, a brief description of commercial STMs and AFMs follows.

Commercial STMs

There are a number of commercial STMs available on the market. Digital Instruments, Inc. located in Santa Barbara, CA introduced the first commercial STM, the Nanoscope I, in 1987. In a recent Nanoscope IV STM for operation in ambient air, the sample is held in position while a piezoelectric crystal in the form of a cylindrical tube (referred to as PZT tube scanner) scans the sharp metallic probe over the surface in a raster pattern while sensing and outputting the tunneling current to the control station, Fig. 1.3. The digital signal processor

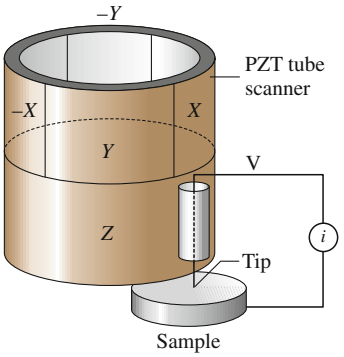

Fig. 1.3 Principle of operation of a commercial STM, a sharp tip attached to a piezoelectric tube scanner is scanned on a sample (From [16])

(DSP) calculates the desired separation of the tip from the sample by sensing the tunneling current flowing between the sample and the tip. The bias voltage applied between the sample and the tip encourages the tunneling current to flow. The DSP completes the digital feedback loop by outputting the desired voltage to the piezoelectric tube. The STM operates in both the "constant height" and "constant current" modes depending on a parameter selection in the control panel. In the constant current mode, the feedback gains are set high, the tunneling tip closely tracks the sample surface, and the variation in the tip height required to maintain constant tunneling current is measured by the change in the voltage applied to the piezo tube. In the constant height mode, the feedback gains are set low, the tip remains at a nearly constant height as it sweeps over the sample surface, and the tunneling current is imaged.

Physically, the Nanoscope STM consists of three main parts: the head which houses the piezoelectric tube scanner for three dimensional motion of the tip and the preamplifier circuit (FET input amplifier) mounted on top of the head for the tunneling current, the base on which the sample is mounted, and the base support, which supports the base and head [16, 21]. The base accommodates samples up to 10 mm by 20 mm and 10 mm in thickness. Scan sizes available for the STM are 0.7 μm × 0.7 μm (for atomic resolution), 12 μm × 12 μm, 75 μm × 75 μm and 125 μm × 125 μm.

The scanning head controls the three dimensional motion of tip. The removable head consists of a piezo tube scanner, about 12.7 mm in diameter, mounted into an invar shell used to minimize vertical thermal drifts because of good thermal match between the piezo tube and the Invar. The piezo tube has separate electrodes for X, Y and Z which are driven by separate drive circuits. The electrode configuration (Fig. 1.3) provides x and y motions which are perpendicular to each other, minimizes horizontal and vertical coupling, and provides good sensitivity. The vertical motion of the tube is controlled by the Z electrode which is driven by the feedback loop. The x and y scanning motions are each controlled by two electrodes which are driven by voltages of same magnitudes, but opposite signs. These electrodes are called $-Y$, $-X$, $+Y$, and $+X$. Applying complimentary voltages allows a short, stiff tube to provide a good scan range without large voltages. The motion of the tip due to external vibrations is proportional to the square of the ratio of vibration frequency to the resonant frequency of the tube. Therefore, to minimize the tip vibrations, the resonant frequencies of the tube are high about 60 kHz in the vertical direction and about 40 kHz in the horizontal direction. The tip holder is a stainless steel tube with a 300 μm inner diameter for 250 μm diameter tips, mounted in ceramic in order to keep the mass on the end of the tube low. The tip is mounted either on the front edge of the tube (to keep mounting mass low and resonant frequency high) (Fig. 1.3) or the center of the tube for large range scanners, namely 75 and 125 μm (to preserve the symmetry of the scanning.) This commercial STM accepts any tip with a 250 μm diameter shaft. The piezotube requires X–Y calibration which is carried out by imaging an appropriate calibration standard. Cleaved graphite is used for the small-scan length head while two dimensional grids (a gold plated ruling) can be used for longer range heads.

The Invar base holds the sample in position, supports the head, and provides coarse *x*–*y* motion for the sample. A spring-steel sample clip with two thumb screws holds the sample in place. An *x*–*y* translation stage built into the base allows the sample to be repositioned under the tip. Three precision screws arranged in a triangular pattern support the head and provide coarse and fine adjustment of the tip height. The base support consists of the base support ring and the motor housing. The stepper motor enclosed in the motor housing allows the tip to be engaged and withdrawn from the surface automatically.

Samples to be imaged with STM must be conductive enough to allow a few nanoamperes of current to flow from the bias voltage source to the area to be scanned. In many cases, nonconductive samples can be coated with a thin layer of a conductive material to facilitate imaging. The bias voltage and the tunneling current depend on the sample. Usually they are set at a standard value for engagement and fine tuned to enhance the quality of the image. The scan size depends on the sample and the features of interest. Maximum scan rate of 122 Hz can be used. The maximum scan rate is usually related to the scan size. Scan rate above 10 Hz is used for small scans (typically 60 Hz for atomic-scale imaging with a 0.7 μm scanner). The scan rate should be lowered for large scans, especially if the sample surfaces are rough or contain large steps. Moving the tip quickly along the sample surface at high scan rates with large scan sizes will usually lead to a tip crash. Essentially, the scan rate should be inversely proportional to the scan size (typically 2–4 Hz for 1 μm, 0.5–1 Hz for 12 μm, and 0.2 Hz for 125 μm scan sizes). Scan rate in length/time, is equal to scan length divided by the scan rate in Hz. For example, for 10 μm × 10 μm scan size scanned at 0.5 Hz, the scan rate is 10 μm/s. The 256 × 256 data formats are most commonly used. The lateral resolution at larger scans is approximately equal to scan length divided by 256.

Commercial AFM

A review of early designs of AFMs is presented by Bhushan [21]. There are a number of commercial AFMs available on the market. Major manufacturers of AFMs for use in ambient environment are: Digital Instruments Inc., a subsidiary of Veeco Instruments, Inc., Santa Barbara, California; Topometrix Corp., a subsidiary of Veeco Instruments, Inc., Santa Clara, California; and other subsidiaries of Veeco Instruments Inc., Woodbury, New York; Molecular Imaging Corp., Phoenix, Arizona; Quesant Instrument Corp., Agoura Hills, California; Nanoscience Instruments Inc., Phoenix, Arizona; Seiko Instruments, Japan; and Olympus, Japan. AFM/STMs for use in UHV environment are primarily manufactured by Omicron Vakuumphysik GMBH, Taunusstein, Germany.

We describe here two commercial AFMs – small sample and large sample AFMs – for operation in the contact mode, produced by Digital Instruments, Inc., Santa Barbara, CA, with scanning lengths ranging from about 0.7 μm (for atomic resolution) to about 125 μm [28–31]. The original design of these AFMs comes from Meyer and Amer [32]. Basically the AFM scans the sample in a raster pattern while

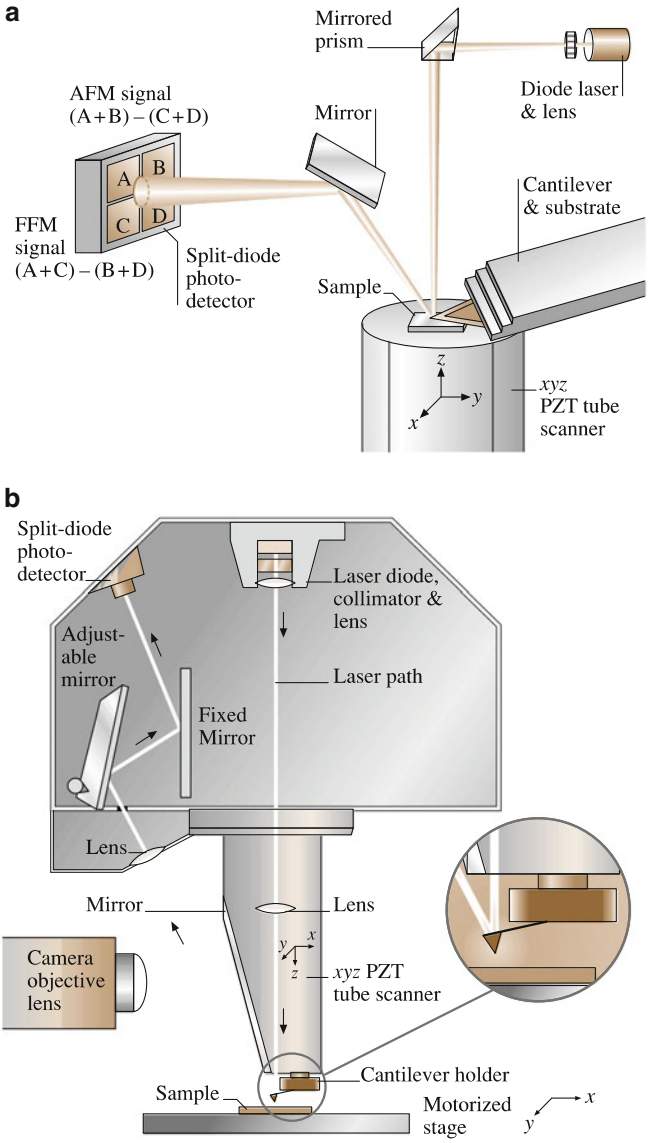

Fig. 1.4 Principles of operation of (**a**) a commercial small sample AFM/FFM, and (**b**) a large sample AFM/FFM (From [16])

outputting the cantilever deflection error signal to the control station. The cantilever deflection (or the force) is measured using laser deflection technique, Fig. 1.4. The DSP in the workstation controls the z-position of the piezo based on the cantilever deflection error signal. The AFM operates in both the "constant height" and "constant

force" modes. The DSP always adjusts the height of the sample under the tip based on the cantilever deflection error signal, but if the feedback gains are low the piezo remains at a nearly "constant height" and the cantilever deflection data is collected. With the high gains, the piezo height changes to keep the cantilever deflection nearly constant (therefore the force is constant) and the change in piezo height is collected by the system.

To further describe the principle of operation of the commercial small sample AFM shown in Fig. 1.4a, the sample, generally no larger than 10 mm × 10 mm, is mounted on a PZT tube scanner which consists of separate electrodes to scan precisely the sample in the *x*-*y* plane in a raster pattern and to move the sample in the vertical (*z*) direction. A sharp tip at the free end of a flexible cantilever is brought in contact with the sample. Features on the sample surface cause the cantilever to deflect in the vertical and lateral directions as the sample moves under the tip. A laser beam from a diode laser (5 mW max peak output at 670 nm) is directed by a prism onto the back of a cantilever near its free end, tilted downward at about 10° with respect to the horizontal plane. The reflected beam from the vertex of the cantilever is directed through a mirror onto a quad photodetector (split photodetector with four quadrants, commonly called position-sensitive detector or PSD, produced by Silicon Detector Corp., Camarillo, California). The differential signal from the top and bottom photodiodes provides the AFM signal which is a sensitive measure of the cantilever vertical deflection. Topographic features of the sample cause the tip to deflect in the vertical direction as the sample is scanned under the tip. This tip deflection will change the direction of the reflected laser beam, changing the intensity difference between the top and bottom sets of photodetectors (AFM signal). In the AFM operating mode called the height mode, for topographic imaging or for any other operation in which the applied normal force is to be kept a constant, a feedback circuit is used to modulate the voltage applied to the PZT scanner to adjust the height of the PZT, so that the cantilever vertical deflection (given by the intensity difference between the top and bottom detector) will remain constant during scanning. The PZT height variation is thus a direct measure of the surface roughness of the sample.

In a large sample AFM, both force sensors using optical deflection method and scanning unit are mounted on the microscope head, Fig. 1.4b. Because of vibrations added by cantilever movement, lateral resolution of this design is somewhat poorer than the design in Fig. 1.4a in which the sample is scanned instead of cantilever beam. The advantage of the large sample AFM is that large samples can be measured readily.

Most AFMs can be used for topography measurements in the so-called tapping mode (intermittent contact mode), also referred to as dynamic force microscopy. In the tapping mode, during scanning over the surface, the cantilever/tip assembly is sinusoidally vibrated by a piezo mounted above it, and the oscillating tip slightly taps the surface at the resonant frequency of the cantilever (70–400 Hz) with a constant (20–100 nm) oscillating amplitude introduced in the vertical direction with a feedback loop keeping the average normal force constant, Fig. 1.5. The oscillating amplitude is kept large enough so that the tip does not get stuck to the

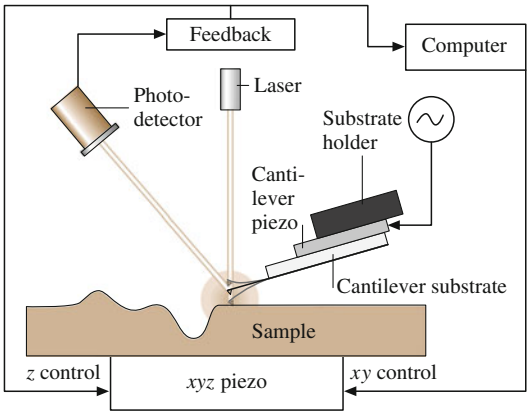

Fig. 1.5 Schematic of tapping mode used for surface roughness measurement (From [16])

sample because of adhesive attractions. The tapping mode is used in topography measurements to minimize effects of friction and other lateral forces and/or to measure topography of soft surfaces.

Topographic measurements are made at any scanning angle. At a first instance, scanning angle may not appear to be an important parameter. However, the friction force between the tip and the sample will affect the topographic measurements in a parallel scan (scanning along the long axis of the cantilever). Therefore a perpendicular scan may be more desirable. Generally, one picks a scanning angle which gives the same topographic data in both directions; this angle may be slightly different than that for the perpendicular scan.

For measurement of friction force being applied at the tip surface during sliding, left hand and right hand sets of quadrants of the photodetector are used. In the so-called friction mode, the sample is scanned back and forth in a direction orthogonal to the long axis of the cantilever beam. A friction force between the sample and the tip will produce a twisting of the cantilever. As a result, the laser beam will be reflected out of the plane defined by the incident beam and the beam reflected vertically from an untwisted cantilever. This produces an intensity difference of the laser beam received in the left hand and right hand sets of quadrants of the photodetector. The intensity difference between the two sets of detectors (FFM signal) is directly related to the degree of twisting and hence to the magnitude of the friction force. This method provides three-dimensional maps of friction force. One problem associated with this method is that any misalignment between the laser beam and the photodetector axis would introduce error in the measurement. However, by following the procedures developed by Ruan and Bhushan [30], in which the average FFM signal for the sample scanned in two opposite directions is subtracted from the friction profiles of each of the two scans, the misalignment effect is eliminated. By following the friction force calibration procedures developed by Ruan and Bhushan [30], voltages corresponding to friction forces can be converted to force unites. The coefficient of friction is obtained from the slope of friction force data measured as a function of normal loads typically ranging from

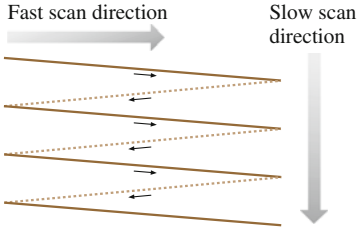

Fig. 1.6 Schematic of triangular pattern trajectory of the AFM tip as the sample is scanned in two dimensions. During imaging, data are recorded only during scans along the solid scan lines (From [16])

10 to 150 nN. This approach eliminates any contributions due to the adhesive forces [33]. For calculation of the coefficient of friction based on a single point measurement, friction force should be divided by the sum of applied normal load and intrinsic adhesive force. Furthermore, it should be pointed out that for a single asperity contact, the coefficient of friction is not independent of load.

The tip is scanned in such a way that its trajectory on the sample forms a triangular pattern, Fig. 1.6. Scanning speeds in the fast and slow scan directions depend on the scan area and scan frequency. Scan sizes ranging from less than 1 nm × 1 nm to 125 μm × 125 μm and scan rates from less than 0.5–122 Hz typically can be used. Higher scan rates are used for smaller scan lengths. For example, scan rates in the fast and slow scan directions for an area of 10 μm × 10 μm scanned at 0.5 Hz are 10 μm/s and 20 nm/s, respectively.

1.4.2 Surface Force Apparatus (SFA)

Surface Force Apparatuses (SFAs) are used to study both static and dynamic properties of the molecularly-thin liquid films sandwiched between two molecularly smooth surfaces. The SFAs were originally developed by Tabor and Winterton [27] and later by Israelachvili and Tabor [34] to measure van der Waals forces between two mica surfaces as a function of separation in air or vacuum. Israelachvili and Adams [35] developed a more advanced apparatus to measure normal forces between two surfaces immersed in a liquid so thin that their thickness approaches the dimensions of the liquid molecules themselves. A similar apparatus was also developed by Klein [36]. The SFAs, originally used in studies of adhesive and static interfacial forces were first modified by Chan and Horn [37] and later by Israelachvili et al. [38] and Klein et al. [39] to measure the dynamic shear (sliding) response of liquids confined between molecularly smooth optically-transparent mica surfaces. Optically transparent surfaces are required because the surface separation is measured using an optical interference technique. Van Alsten and Granick [40] and Peachey et al. [41] developed a new friction attachment which allow for the two surfaces to be sheared past each other at varying sliding speeds or oscillating frequencies while simultaneously measuring both the friction force and normal force between them. Israelachvili [42] and Luengo et al. [43] also presented modified SFA designs for dynamic measurements including friction at oscillating

frequencies. Because the mica surfaces are molecularly smooth, the actual area of contact is well defined and measurable, and asperity deformation do not complicate the analysis. During sliding experiments, the area of parallel surfaces is very large compared to the thickness of the sheared film and this provides an ideal condition for studying shear behavior because it permits one to study molecularly-thin liquid films whose thickness is well defined to the resolution of an angstrom. Molecularly thin liquid films cease to behave as a structural continuum with properties different from that of the bulk material [40, 44–47].

Tonck et al. [48] and Georges et al. [49] developed a SFA used to measure the static and dynamic forces (in the normal direction) between a smooth fused borosilicate glass against a smooth and flat silicon wafer. They used capacitance technique to measure surface separation; therefore, use of optically-transparent surfaces was not required. Among others, metallic surfaces can be used at the interface. Georges et al. [50] modified the original SFA so that a sphere can be moved towards and away from a plane and can be sheared at constant separation from the plane, for interfacial friction studies.

For a detailed review of various types of SFAs, see Israelachvili [42, 51], Horn [52], and Homola [53]. SFAs based on their design are commercially available from SurForce Corporation, Santa Barbara, California.

Israelachvili's and Granick's Design

Following review is primarily based on the papers by Israelachvili [42] and Homola [53]. Israelachvili et al.'s design later followed by Granick et al. for oscillating shear studies, is most commonly used by researchers around the world.

Classical SFA The classical apparatus developed for measuring equilibrium or static intersurface forces in liquids and vapors by Israelachvili and Adams [35], consists of a small, air-tight stainless steel chamber in which two molecularly smooth curved mica surfaces can be translated towards or away from each other, see Fig. 1.7. The distance between the two surfaces can also be independently controlled to within ± 0.1 nm and the force sensitivity is about 10 nN. The technique utilizes two molecularly smooth mica sheets, each about 2 μm thick, coated with a semi reflecting 50–60 nm layer of pure silver, glued to rigid cylindrical silica disks of radius about 10 mm (silvered side down) mounted facing each other with their axes mutually at right angles (crossed cylinder position), which is geometrically equivalent to a sphere contacting a flat surface. The adhesive glue which is used to affix the mica to the support is sufficiently compliant, so the mica will flatten under the action of adhesive forces or applied load to produce a contact zone in which the surfaces are locally parallel and planar. Outside of this contact zone the separation between surfaces increases and the liquid, which is effectively in a bulk state, makes a negligible contribution to the overall response. The lower surface is supported on a cantilever spring which is used to push the two surfaces together with a known load. When the surfaces are forced into contact, they flatten elastically so that the contact zone is circular for duration of the static or sliding

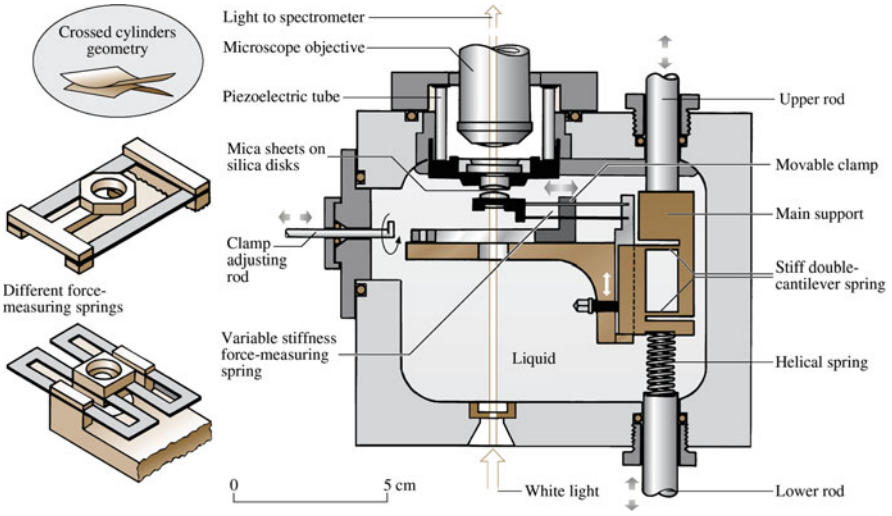

Fig. 1.7 Schematic of the surface force apparatus that employs the cross cylinder geometry [35, 42]

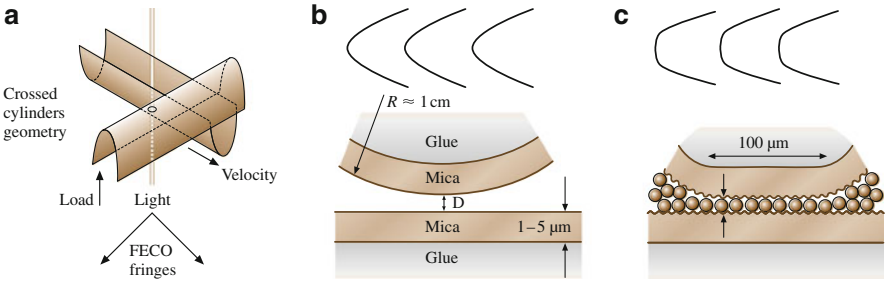

Fig. 1.8 (**a**) Cross cylinder configuration of mica sheet, showing formation of contact area. Schematic of the fringes of equal chromatic order (FECO) observed when two mica surfaces are (**b**) separated by distance D and (**c**) are flattened with a monolayer of liquid between them [54]

interactions. The surface separation is measured using optical interference fringes of equal chromatic order (FECO) which enables the area of molecular contact and the surface separation to be measured to within 0.1 nm. For measurements, white light is passed vertically up through the two mica surfaces and the emerging beam is then focused onto the slit of a grating spectrometer. From the positions and shapes of the colored FECO fringes in the spectrogram, the distance between the two surfaces and the exact shape of the two surfaces can be measured (as illustrated in Fig. 1.8), as can the refractive index of the liquid (or material) between them. In particular, this allows for reasonably accurate determinations of the quantity of material deposited or adsorbed on the surfaces and the area of contact between two molecularly smooth surfaces. Any changes may be readily observed in both static

and sliding conditions in real time (applicable to the design shown in Fig. 1.8) by monitoring the changing shapes of these fringes.

The distance between the two surfaces is controlled by use of a three-stage mechanism of increasing sensitivity: coarse control (upper rod) allows positioning of within about 1 μm, the medium control (lower rod, which depresses the helical spring and which in turn, bends the much stiffer double-cantilever spring by 1/1,000 of this amount) allows positioning to about 1 nm, and the piezoelectric crystal tube – which expands or controls vertically by about 0.6 nm/V applied axially across the cylindrical wall – is used for final positioning to 0.1 nm.

The normal force is measured by expanding or contracting the piezoelectric crystal by a known amount and then measuring optically how much the two surfaces have actually moved; any difference in the two values when multiplied by the stiffness of the force measuring spring gives the force difference between the initial and final positions. In this way both repulsive and attractive forces can be measured with a sensitivity of about 10 nN. The force measuring springs can be either single-cantilever or double-cantilever fixed-stiffness springs (as shown in Fig. 1.7), or the spring stiffness can be varied during an experiment (by up to a factor of 1,000) by shifting the position of the dovetailed clamp using the adjusting rod. Other spring attachments, two of which are shown at the top of the figure, can replace the variable stiffness spring attachment (top right: nontilting nonshearing spring of fixed stiffness). Each of these springs are interchangeable and can be attached to the main support, allowing for greater versatility in measuring strong or weak and attractive or repulsive forces. Once the force F as a function of distance D is known for the two surfaces of radius R, the force between any other curved surfaces simply scales by R. Furthermore, the adhesion energy (or surface or interfacial free energy) E per unit area between two flat surfaces is simply related to F by the so-called Derjaguin approximation [51] $E = F/2\pi R$. We note that SFA is one of the few techniques available for directly measuring equilibrium force-laws (i.e., force versus distance at constant chemical potential of the surrounding solvent medium) [42]. The SFA allows for both weak or strong and attractive or repulsive forces.

Mostly the molecularly smooth surface of mica is used in these measurements [55], however, silica [56] and sapphire [57] have also been used. It is also possible to deposit or coat each mica surface with metal films [58, 59], carbon and metal oxides [60], adsorbed polymer layers [61], surfactant monolayers and bilayers [51, 58, 62, 63]. The range of liquids and vapors that can be used is almost endless.

Sliding Attachments for Tribological Studies So far we have described a measurement technique which allows measurements of the normal forces between surfaces, that is, those occurring when two surfaces approach or separate from each other. However, in tribological situations, it is the transverse or shear forces that are of primary interest when two surfaces slide past each other. There are essentially two approaches used in studying the shear response of confined liquid films. In the first approach (constant velocity friction or steady-shear attachment), the friction is measured when one of the surfaces is traversed at a constant speed over a distance of several hundreds of microns [38, 39, 45, 54, 60, 64, 65]. The second approach (oscillatory shear attachment) relies on the measurement of viscous dissipation and

elasticity of confined liquids by using periodic sinusoidal oscillations over a range of amplitudes and frequencies [40, 41, 44, 66, 67].

For the constant velocity friction (steady-shear) experiments, the surface force apparatus was outfitted with a lateral sliding mechanism [38, 42, 46, 54, 64, 65] allowing measurements of both normal and shearing forces (Fig. 1.9). The piezoelectric crystal tube mount supporting the upper silica disk of the basic apparatus shown in Fig. 1.7, is replaced. Lateral motion is initiated by a variable speed motor-driven micrometer screw that presses against the translation stage, which is connected via two horizontal double-cantilever strip springs to the rigid mounting plate. The translation stage also supports two vertical double-cantilever springs (Fig. 1.10) that at their lower end are connected to a steel plate supporting the upper silica disk. One of the vertical springs acts as a frictional force detector by having four resistance strain gages attached to it, forming the four arms of a Wheatstone bridge and electrically connected to a chart recorder. Thus, by rotating the micrometer,

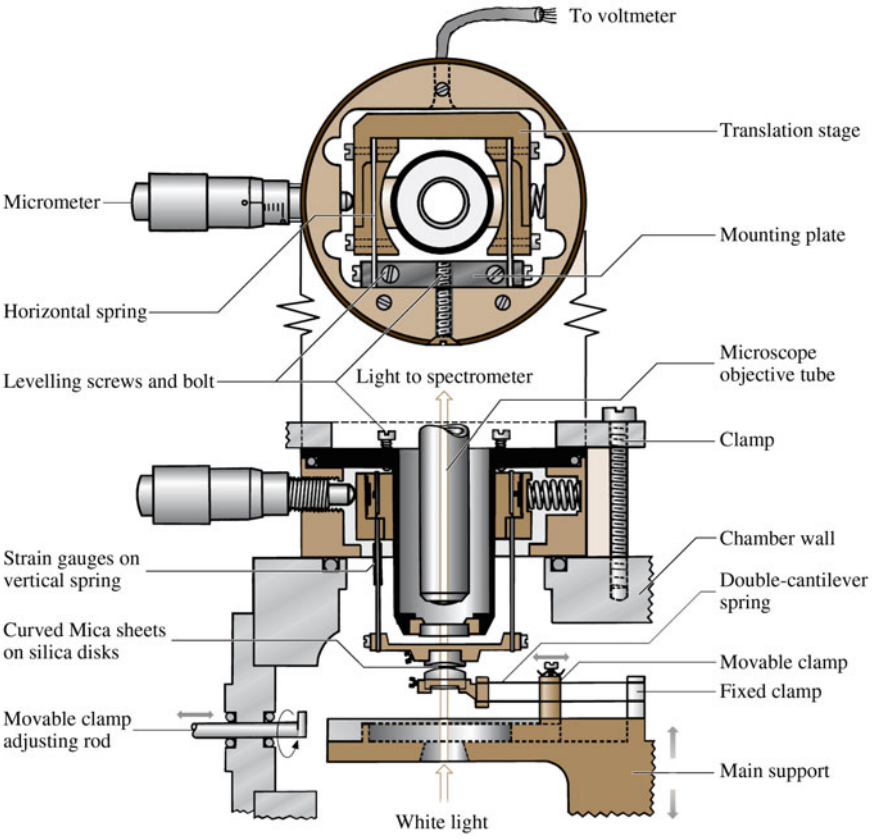

Fig. 1.9 Schematic of shear force apparatus. Lateral motion is initiated by a variable speed motor-driven micrometer screw that presses against the translation stage which is connected through two horizontal double-cantilever strip springs to the rigid mounting plate [38, 42]

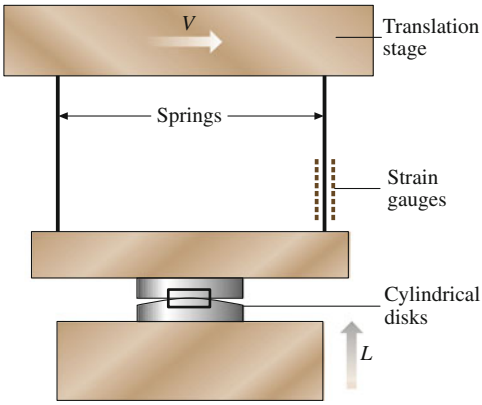

Fig. 1.10 Schematic of the sliding attachment. The translation stage also supports two vertical double-cantilever springs, which at their lower end are connected to a steel plate supporting the upper silica disk [46]

the translation stage deflects, causing the upper surface to move horizontally and linearly at a steady rate. If the upper mica surface experiences a transverse frictional or viscous shearing force, this will cause the vertical springs to deflect, and this deflection can be measured by the strain gages. The main support, force-measuring double-cantilever spring, movable clamp, white light, etc., are all parts of the original basic apparatus (Fig. 1.7), whose functions are to control the surface separation, vary the externally applied normal load, and measure the separation and normal force between the two surfaces, as already described. Note that during sliding, the distance between the surfaces, their true molecular contact area, their elastic deformation, and their lateral motion can all be simultaneously monitored by recording the moving FECO fringe pattern using a video camera and recording it on a tape [46].

The two surfaces can be sheared past each other at sliding speeds which can be varied continuously from 0.1 to 20 μm/s while simultaneously measuring both the transverse (frictional) force and the normal (compressive or tensile) force between them. The lateral distances traversed are on the order of a several hundreds of micrometers which correspond to several diameters of the contact zone.

With an oscillatory shear attachment, developed by Granick et al., viscous dissipation and elasticity and dynamic viscosity of confined liquids by applying periodic sinusoidal oscillations of one surface with respect to the other can be studied [40, 41, 44, 66, 67]. This attachment allows for the two surfaces to be sheared past each other at varying sliding speeds or oscillating frequencies while simultaneously measuring both the transverse (friction or shear) force and the normal load between them. The externally applied load can be varied continuously, and both positive and negative loads can be applied. Finally the distance between the surfaces, their true molecular contact area, their elastic (or viscoelastic) deformation and their lateral motion can all be simultaneously by recording the moving interference fringe pattern using a video camera-recorder system.

To produce shear while maintaining constant film thickness or constant separation of the surfaces, the top mica surface is suspended from the upper portion of the apparatus by two piezoelectric bimorphs. A schematic description of the surface force apparatus with the installed shearing device is shown in Fig. 1.11 [40, 41, 44, 66, 67].

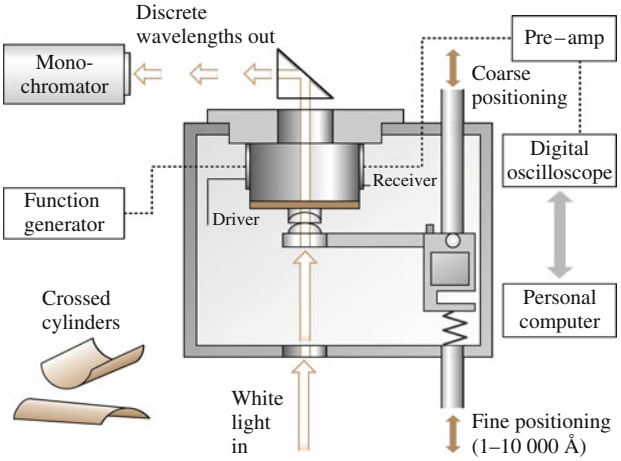

Fig. 1.11 Schematic of the oscillatory shearing apparatus [40]

Israelachvili [42] and Luengo et al. [43] have also presented similar designs. The lower mica surface, as in the steady-shear sliding attachment, is stationary and sits at the tip of a double cantilever spring attached at the other end to a stiff support. The externally applied load can be varied continuously by displacing the lower surface vertically. An AC voltage difference applied by a signal generator (driver) across one of the bimorphs tends to bend it in oscillatory fashion while the frictional force resists that motion. Any resistance to sliding induces an output voltage across the other bimorphs (receiver) which can be easily measured by a digital oscilloscope. The sensitivity in measuring force is on the order of a few μN and the amplitudes of measured lateral displacement can range from a few nm to 10 μm. The design is flexible and allows to induce time-varying stresses with different characteristic wave shapes simply by changing the wave form of the input electrical signal. For example, when measuring the apparent viscosity, a sine wave input is convenient to apply. Figure 1.12a shows an example of the raw data, obtained with a hexadecane film at a moderate pressure, when a sine wave was applied to one of the bimorphs [66]. By comparing the calibration curve with the response curve, which was attenuated in amplitude and lagged in phase, an apparent dynamic viscosity can be inferred. On the other hand, a triangular waveform is more suitable when studying the yield stress behavior of solid-like films as of Fig. 1.12b. The triangular waveform, showing a linear increase and decrease of the applied force with time, is proportional to the driving force acting on the upper surface. The response waveform, which represents a resistance of the interface to shear, remains very small indicating that the surfaces are in a stationary contact with respect to each other until the applied stress reaches a yield point. At the yield point the slope of the response curve increases dramatically, indicating the onset of sliding.

Homola [53] compared the two approaches – steady shear attachment and oscillating shear attachment. In experiments conducted by Israelachvili and his

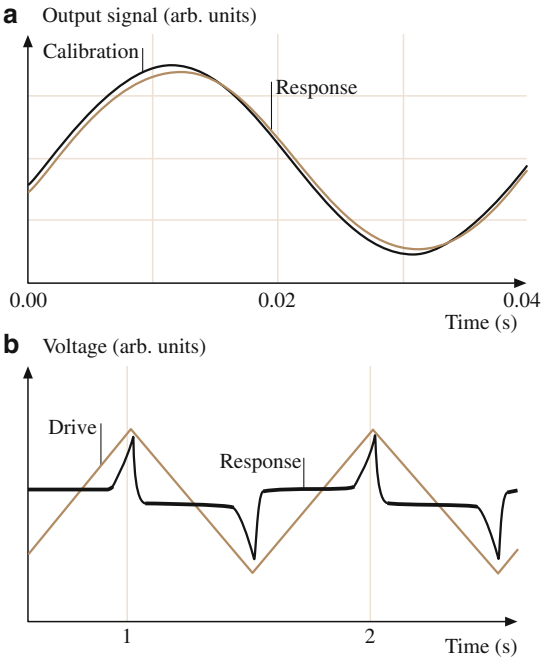

Fig. 1.12 (**a**) Two output signals induced by an applied sine wave (not shown) are displaced. The "calibration" waveform is obtained with the mica sheets completely separated. The response waveform is obtained with a thin liquid film between the sheets, which causes it to lag the calibration waveform, (**b**) the oscilloscope trace of the drive and response voltages used to determine critical shear stress. The drive waveform shows voltage proportional to induced stress on the sheared film and the response waveform shows voltage proportional to resulting velocity. Spikes in the response curve correspond to the stick–slip event [66]

co-workers, the steady-shear attachment was employed to focus on the dynamic frictional behavior of the film after a sufficiently high shear stress was applied to exceed the yield stress and to produce sliding at a constant velocity. In these measurements, the film was subjected to a constant shearing force for a time sufficiently long to allow them to reach a dynamic equilibrium, i.e., the molecules, within the film, had enough time to order and align with respect to the surface, both normally and tangentially. Under these conditions, dynamic friction was observed to be "quantized" according to the number of liquid layers between the solid surfaces and independent of the shear rate [38]. Clearly, in this approach, the molecular ordering is optimized by a steady shear which imposes a preferred orientation on the molecules in the direction of shear.

The above mode of sliding is particularly important when the sheared film is made of a long chain lubricant molecules requiring a significantly long sliding time to order and align and even a longer time to relax (disorder) when sliding stops. This suggests that a steady-state friction is realized only when the duration of sliding exceeds the time required for an ensemble of the molecules to fully order in a

specific shear field. It also suggests, that static friction should depend critically on the sliding time and the extend of the shear induced ordering [53].

In contrast, the oscillatory shear method, which utilizes periodic sinusoidal oscillations over a range of amplitudes and frequencies, addresses a response of the system to rapidly varying strain rates and directions of sliding. Under these conditions, the molecules, especially those exhibiting a solid-like behavior, cannot respond sufficiently fast to stress and are unable to order fully during duration of a single pass, i.e., their dynamic and static behavior reflects and oscillatory shear induced ordering which might or might not represent an equilibrium dynamic state. Thus, the response of the sheared film will depend critically on the conditions of shearing, i.e., the strain, the pressure, and the sliding conditions (amplitude and frequency of oscillations) which in turn will determine a degree of molecular ordering. This may explain the fact that the layer structure and "quantization" of the dynamic and static friction was not observed in these experiments in contrast to results obtained when velocity was kept constant. Intuitively, this behavior is expected considering that the shear-ordering tendency of the system is frequently disturbed by a shearing force of varying magnitude and direction. Nonetheless, the technique is capable of providing an invaluable insight into the shear behavior of molecularly thin films subjected to non-linear stresses as it is frequently encountered in practical applications. This is especially true under conditions of boundary lubrication where interacting surface asperities will be subjected to periodic stresses of varying magnitudes and frequencies [53].

Georges et al.'s Design

The SFA developed by Tonck et al. [48] and Georges et al. [49] to measure static and dynamic forces in the normal direction, between surfaces in close proximity, is shown in Fig. 1.13. In their apparatus, a drop of liquid is introduced between a macroscopic spherical body and a plane. The sphere is moved towards and away from a plane using the expansion and the vibration of a piezoelectric crystal. Piezoelectric crystal is vibrated at low amplitude around an average separation for dynamic measurements to provide dynamic function of the interface. The plane specimen is supported by a double-cantilever spring. Capacitance sensor C_1 measures the elastic deformation of the cantilever and thus the force transmitted through the liquid to the plane. Second capacitance sensor C_2 is designed to measure the relative displacement between the supports of the two solids. The reference displacement signal is the sum of two signals: first, a ramp provides a constant normal speed from 50 to 0.01 nm/s, and, second, the piezoelectric crystal is designed to provide a small sinusoidal motion, in order to determine the dynamic behavior of sphere-plane interactions. A third capacitance sensor C measures the electrical capacitance between the sphere and the plane. In all cases, the capacitance is determined by incorporating the signal of an oscillator in the inductive–capacitance (*L–C*) resonant input stage of an oscillator to give a signal-dependent frequency in the range of 5–12 MHz. The resulting fluctuations in oscillation frequency are detected using a low noise frequency discriminator.

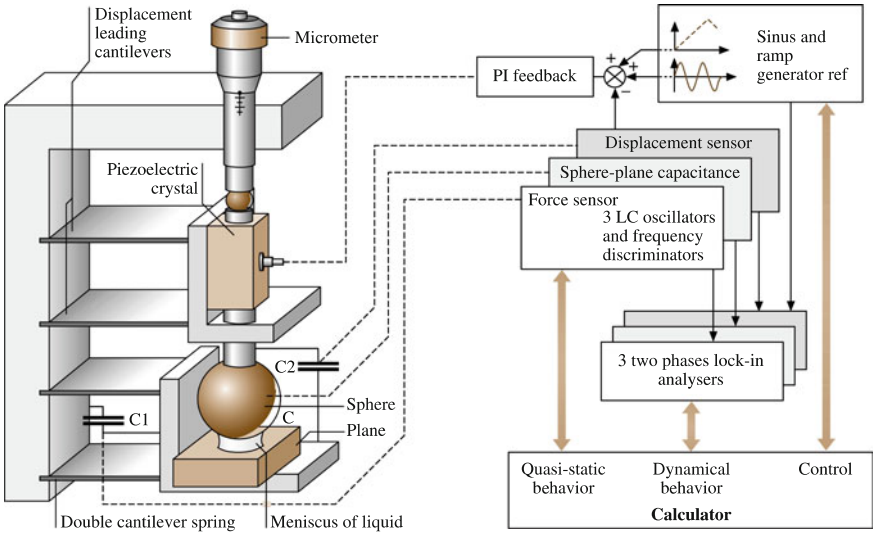

Fig. 1.13 Schematic of the surface force apparatus that employs a sphere–plane arrangement [49]

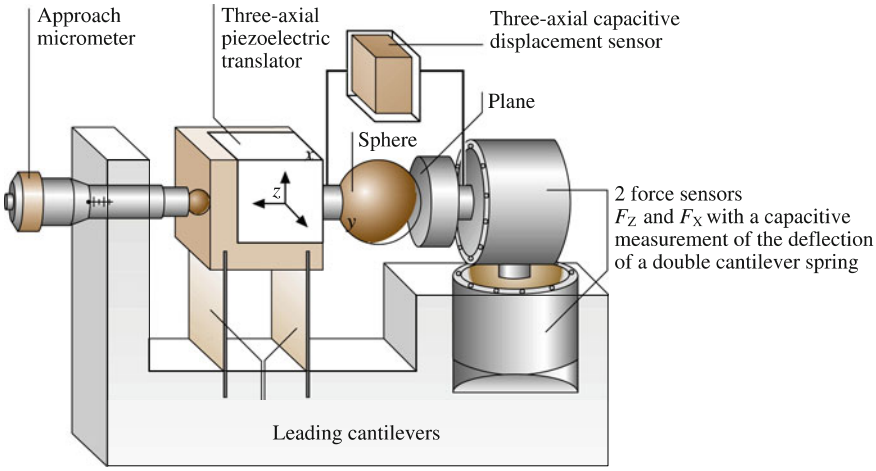

Fig. 1.14 Schematic of shear force apparatus [50]

Simultaneous measurements of sphere-plane displacement, surface force, and the damping of the interface allows an analysis of all regimes of the interface [49]. Loubet et al. [68] used SFA in the crossed-cylinder geometry using two freshly-cleaved mica sheets similar to the manner used by Israelachvili and coworkers.

Georges et al. [50] modified their original SFA to measure friction forces. In this apparatus, in addition to having sphere move normal to the plane, sphere can be sheared at constant separation from the plane. The shear force apparatus is shown in Fig. 1.14. Three piezoelectric elements controlled by three capacitance sensors

permit accurate motion control and force measurement along three orthogonal axes with displacement sensitivity of 10^{-3} nm and force sensitivity of 10^{-8} N. Adhesion and normal deformation experiments are conducted in the normal approach (z-axis). Friction experiments are conducted by introducing displacement in the X-direction at a constant normal force. In one of the experiment, Georges et al. [50] used 2.95 mm diameter sphere made of cobalt-coated fused borosilicate glass and a silicon wafer for the plane.

1.4.3 Vibration Isolation

STM, AFM and SFA should be isolated from sources of vibration in the acoustic and sub-acoustic frequencies especially for atomic-scale measurements. Vibration isolation is generally provided by placing the instrument on a vibration isolation air table. For further isolation, the instrument should be placed on a pad of soft silicone rubber. A cheaper alternative consists of a large mass of 100 N or more, suspended from elastic "bungee" cords. The mass should stretch the cords at least 0.3 m, but not so much that the cords reach their elastic limit. The instrument should be placed on the large mass. The system, including the microscope, should have a natural frequency of about 1 Hz or less both vertically and horizontally. Test this by gently pushing on the mass and measure the rate at which its swings or bounces.

1.5 Magnetic Storage Devices and MEMS/NEMS

1.5.1 Magnetic Storage Devices

Magnetic storage devices used for storage and retrieval are tape, flexible (floppy) disk and rigid disk drives. These devices are used for audio, video and data storage applications. Magnetic storage industry is some $ 60 billion a year industry with $ 20 billion for audio and video recording (almost all tape drives/media) and $ 40 billion for data storage. In the data storage industry, magnetic rigid disk drives/media, tape drives/media, flexible disk drives/media, and optical disk drive/media account for about $ 25 B, $ 6 B, $ 3 B, and $ 6 B, respectively. Magnetic recording and playback involves the relative motion between a magnetic medium (tape or disk) against a read-write magnetic head. Heads are designed so that they develop a (load-carrying) hydrodynamic air film under steady operating conditions to minimize head–medium contact. However, physical contact between the medium and head occurs during starts and stops, referred to as contact-start-stops (CSS) technology [13, 14, 69]. In the modern magnetic storage devices, the flying heights (head-to-medium separation) are on the order of 5–20 nm and roughnesses of head and medium surfaces are on the order of 1–2 nm RMS. The need for ever-increasing

recording densities requires that surfaces be as smooth as possible and the flying heights be as low as possible. High stiction (static friction) and wear are the limiting technology to future of this industry. Head load/unload (L/UL) technology has recently been used as an alternative to CSS technology in rigid disk drives that eliminates stiction and wear failure mode associated with CSS. Several contact or near contact recording devices are at various stages of development. High stiction and wear are the major impediments to the commercialization of the contact recording.

Magnetic media fall into two categories: particulate media, where magnetic particles (γ-Fe_2O_3, Co-γFe_2O_3, CrO_2, Fe or metal (MP), or barium ferrite) are dispersed in a polymeric matrix and coated onto a polymeric substrate for flexible media (tape and flexible disks); thin-film media, where continuous films of magnetic materials are deposited by vacuum deposition techniques onto a polymer substrate for flexible media or onto a rigid substrate (typically aluminium and more recently glass or glass ceramic) for rigid disks. The most commonly used thin magnetic films for tapes are evaporated Co–Ni (82–18 at.%) or Co–O dual layer. Typical magnetic films for rigid disks are metal films of cobalt-based alloys (such as sputtered Co–Pt–Ni, Co–Ni, Co–Pt–Cr, Co–Cr and Co–NiCr). For high recording densities, trends have been to use thin-film media. Magnetic heads used to date are either conventional thin-film inductive, magnetoresistive (MR) and giant MR (GMR) heads. The air-bearing surfaces (ABS) of tape heads are generally cylindrical in shape. For dual-sided flexible-disk heads, two heads are either spherically contoured and slightly offset (to reduce normal pressure) or are flat and loaded against each other. The rigid-disk heads are supported by a leaf spring (flexure) suspension. The ABS of heads are almost made of Mn–Zn ferrite, Ni–Zn ferrite, Al_2O_3–TiC and calcium titanate. The ABS of some conventional heads are made of plasma sprayed coatings of hard materials such as Al_2O_3–TiO_2 and ZrO_2 [13, 14, 69].

Figure 1.15 shows the schematic illustrating the tape path with details of tape guides in a data-processing linear tape drive (IBM LTO Gen1) which uses a rectangular tape cartridge. Figure 1.16a shows the sectional views of particulate and thin-film magnetic tapes. Almost exclusively, the base film is made of

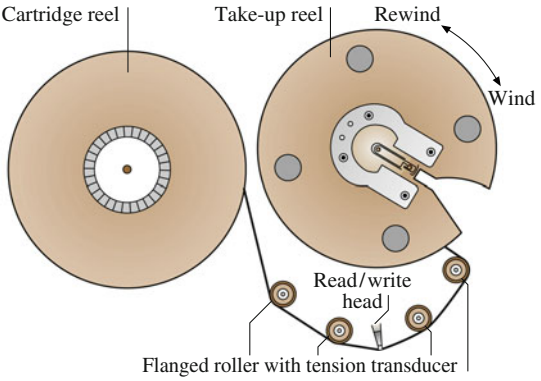

Fig. 1.15 Schematic of tape path in an IBM Linear Tape Open (*LTO*) tape drive

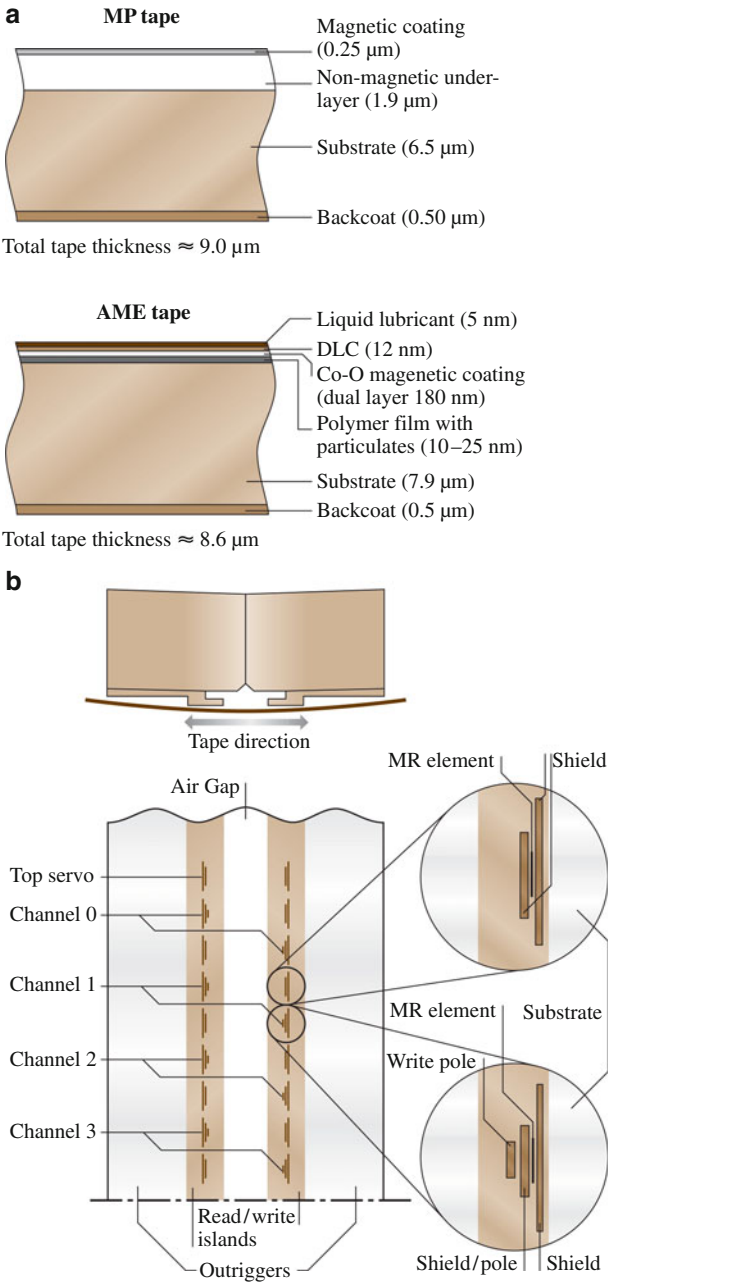

Fig. 1.16 (**a**) Sectional views of particulate and thin-film magnetic tapes, and (**b**) schematic of a magnetic thin-film read/write head for an IBM LTO Gen 1 tape drive

semicrystalline biaxially-oriented poly (ethylene terephthalate) (or PET) or poly (ethylene 2,6 naphthalate) (or PEN) or Aramid. The particulate coating formulation consists of binder (typically polyester polyurethane), submicron accicular shaped magnetic particles (about 50 nm long with an aspect ratio of about 5), submicron head cleaning agents (typically alumina) and lubricant (typically fatty acid ester). For protection against wear and corrosion and low friction/stiction, the thin-film tape is first coated with a diamondlike carbon (DLC) overcoat deposited by plasma enhanced chemical vapor deposition, topically lubricated with primarily a perfluoropolyether lubricant. Figure 1.16b shows the schematic of an eight-track (along with two servo tracks) thin-film read-write head with MR read and inductive write. The head steps up and down to provide 384 total data tracks across the width of the tape. The ABS is made of Al_2O_3–TiC. A tape tension of about 1 N over a 12.7 mm wide tape (normal pressure $\approx$ 14 kPa) is used during use. The RMS roughnesses of ABS of the heads and tape surfaces typically are 1–1.5 nm and 5–8 nm, respectively.

Figure 1.17 shows the schematic of a data processing rigid disk drive with 21.6, 27.4, 48, 63.5, 75, and 95 mm form factor. Nonremovable stack of multiple disks mounted on a ball bearing or hydrodynamic spindle, are rotated by an electric motor at constant angular speed ranging from about 5,000 to in excess of 15,000 RPM, dependent upon the disk size. Head slider-suspension assembly (allowing one slider for each disk surface) is actuated by a stepper motor or a voice coil motor using a rotary actuator. Figure 1.18a shows the sectional views of a thin-film rigid disk. The substrate for rigid disks is generally a non heat-treatable aluminium–magnesium alloy 5086, glass or glass ceramic. The protective overcoat commonly used for thin-film disks is sputtered DLC, topically lubricated with perfluoropolyether type of lubricants. Lubricants with polar-end groups are generally used for thin-film disks in order to provide partial chemical bonding to the overcoat surface. The disks used for CSS technology are laser textured in the landing zone. Figure 1.18b shows the schematic of two thin-film head picosliders with a step at the leading edge, and GMR read and inductive write. "Pico" refers to the small sizes of 1.25 mm $\times$ 1 mm. These sliders use Al_2O_3–TiC (70–30 wt%) as the substrate material with

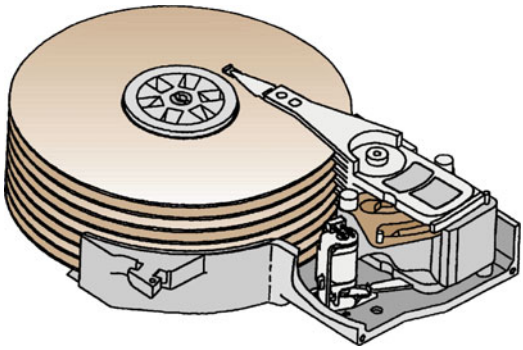

Fig. 1.17 Schematic of a data-processing magnetic rigid disk drive

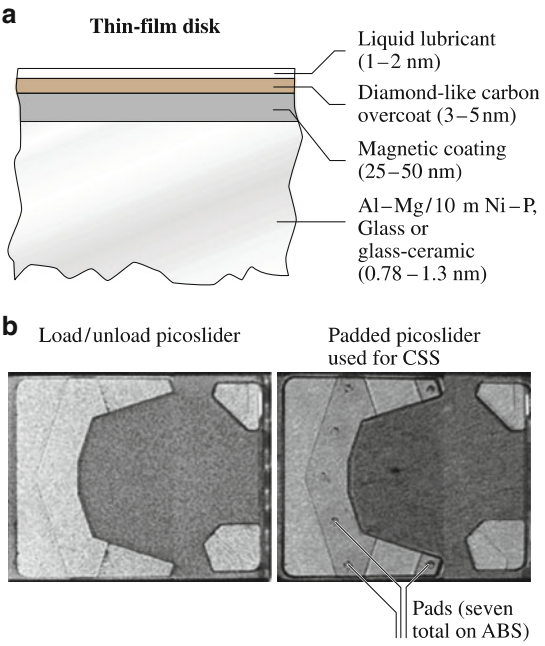

Fig. 1.18 (**a**) Sectional views of a thin-film magnetic rigid disk, and (**b**) schematic of two picosliders – load/unload picoslider and padded picoslider used for CSS

multilayered thin-film head structure coated and with about 3.5 nm thick DLC coating to prevent the thin film structure from electrostatic discharge. The seven pads on the padded slider are made of DLC and are about 40 μm in diameter and 50 nm in height. A normal load of about 3 g is applied during use.

1.5.2 MEMS/NEMS

The advances in silicon photolithographic process technology led to the development of MEMS in the mid-1980s [16]. More recently, lithographic and nonlithographic processes have been developed to process nonsilicon (plastics or ceramics) materials. MEMS for mechanical applications include acceleration, pressure, flow, and gas sensors, linear and rotary actuators, and other microstructures of microcomponents such as electric motors, gear trains, gas turbine engines, nozzles, fluid pumps, fluid valves, switches, grippers, and tweezers. MEMS for chemical applications include chemical sensors and various analytical instruments. Microoptoelectromechanical systems (or MOEMS) include micromirror arrays and fiber optic connectors. Radio frequency MEMS or RF-MEMS include inductors, capacitors, and antennas. High-aspect ratio MEMS (HARMEMS) have also been introduced. BioMEMS include biofluidic chips (microfluidic chips or bioflips or simple biochips) for chemical and biochemical analyses (biosensors in medical diagnostics,

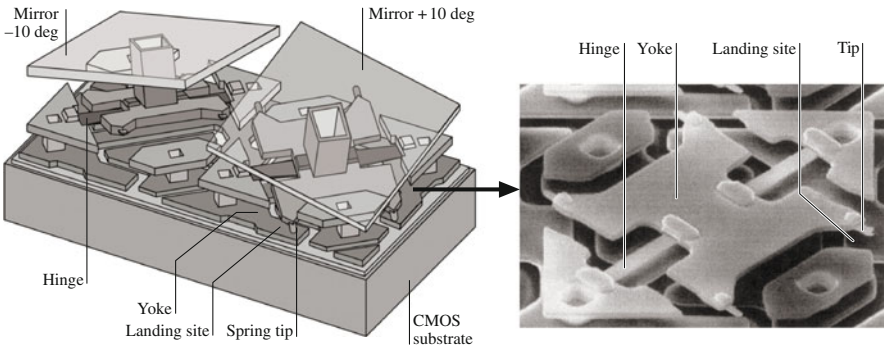

Fig. 1.19 Digital micromirror devices for projection displays (From [16])

e.g., DNA, RNA, proteins, cells, blood pressure and assays, and toxin identification), and implantable drug delivery. Killer applications include capacitive-type silicon accelerometers for automotive sensory applications and digital micromirror devices for projection displays. Any component requiring relative motions needs to be optimized for stiction and wear [16, 20, 22, 69, 70].

Figure 1.19 also shows two digital micromirror device (DMD) pixels used in digital light processing (DLP) technology for digital projection displays in portable and home theater projectors as well as table top and projection TVs [16, 71, 72]. The entire array (chip set) consists of a large number of rotatable aluminium micromirrors (digital light switches) which are fabricated on top of a CMOS static random access memory integrated circuit. The surface micromachined array consists of half of a million to more than two million of these independently controlled reflective, micromirrors (mirror size on the order of 14 μm × 14 μm and 15 μm pitch) which flip backward and forward at a frequency of on the order of 5,000 times a second. For the binary operation, micromirror/yoke structure mounted on torsional hinges is rotated $\pm 10^\circ$ (with respect to the horizontal plane) as a result of electrostatic attraction between the micromirror structure and the underlying memory cell, and is limited by a mechanical stop. Contact between cantilevered spring tips at the end of the yoke (four present on each yoke) with the underlying stationary landing sites is required for true digital (binary) operation. Stiction and wear during a contact between aluminium alloy spring tips and landing sites, hinge memory (metal creep at high operating temperatures), hinge fatigue, shock and vibration failure, and sensitivity to particles in the chip package and operating environment are some of the important issues affecting the reliable operation of a micromirror device. Perfluorodecanoic acid (PFDA) self-assembled monolayers are used on the tip and landing sites to reduce stiction and wear. The spring tip is used in order to use the spring stored energy to pop up the tip during pull-off. A lifetime estimate of over 100,000 operating hours with no degradation in image quality is the norm.

NEMS are produced by nanomachining in a typical top-down approach (from large to small) and bottom-up approach (from small to large) largely relying on nanochemistry [16]. The top-down approach relies on fabrication methods

including advanced integrated-circuit (IC) lithographic methods – electron-beam lithography, and STM writing by removing material atom by atom. The bottom-up approach includes chemical synthesis, the spontaneous "self-assembly" of molecular clusters (molecular self-assembly) from simple reagents in solution, or biological molecules (e.g., DNA) as building blocks to produce three dimensional nanostructures, quantum dots (nanocrystals) of arbitrary diameter (about 10–10^5 atoms), molecular beam epitaxy (MBE) and organometallic vapor phase epitaxy (OMVPE) to create specialized crystals one atomic or molecular layer at a time, and manipulation of individual atoms by an atomic force microscope or atom optics. The self-assembly must be encoded, that is, one must be able to precisely assemble one object next to another to form a designed pattern. A variety of nonequilibrium plasma chemistry techniques are also used to produce layered nanocomposites, nanotubes, and nanoparticles. NEMS field, in addition to fabrication of nanosystems, has provided impetus to development of experimental and computation tools.

Examples of NEMS include nanocomponents, nanodevices, nanosystems, and nanomaterials such as microcantilever with integrated sharp nanotips for STM and AFM, AFM array (Millipede) for data storage, AFM tips for nanolithography, dip-pen nanolithography for printing molecules, biological (DNA) motors, molecular gears, molecularly-thick films (e.g., in giant magnetioresistive or GMR heads and magnetic media), nanoparticles (e.g., nanomagnetic particles in magnetic media), nanowires, carbon nanotubes, quantum wires (QWRs), quantum boxes (QBs), and quantum transistors [16]. BIONEMS include nanobiosensors – microarray of silicon nanowires, roughly few nm in size, to selectively bind and detect even a single biological molecule such as DNA or protein by using nanoelectronics to detect the slight electrical charge caused by such binding, or a microarray of carbon nanotubes to electrically detect glucose, implantable drug-delivery devices – e.g., micro/nanoparticles with drug molecules encapsulated in functionized shells for a site-specific targeting applications, and a silicon capsule with a nanoporous membrane filled with drugs for long term delivery, nanodevices for sequencing single molecules of DNA in the Human Genome Project, cellular growth using carbon nanotubes for spinal cord repair, nanotubes for nanostructured materials for various applications such as spinal fusion devices, organ growth, and growth of artificial tissues using nanofibers.

Figure 1.20 shows AFM based nanoscale data storage system for ultrahigh density magnetic recording which experiences tribological problems [73]. The system uses arrays of several thousand silicon microcantilevers ("Millipede") for thermomechanical recording and playback on an about 40-nm thick polymer (PMMA) medium with a harder Si substrate. The cantilevers are integrated with integrated tip heaters with tips of nanoscale dimensions. Thermomechanical recording is a combination of applying a local force to the polymer layer and softening it by local heating. The tip heated to about 400°C is brought in contact with the polymer for recording. Imaging and reading are done using the heater cantilever, originally used for recording, as a thermal readback sensor by exploiting its temperature-dependent resistance. The principle of thermal sensing is based on the fact that the thermal conductivity between the heater and the storage substrate changes according to the spacing between them. When the spacing between the

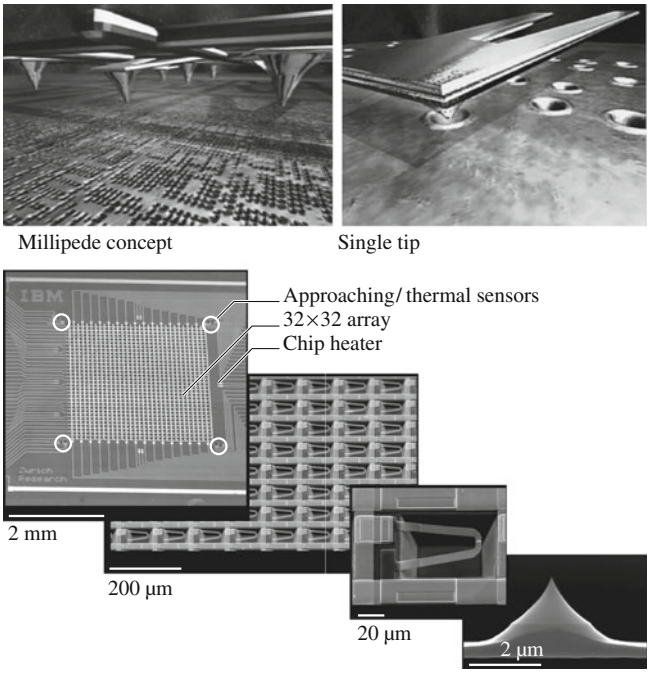

Fig. 1.20 AFM based nanoscale data storage system with 32 × 32 tip array – that experiences a tribological problem (From [16])

heater and sample is reduced as the tip moves into a bit, the heater's temperature and hence its resistance will decrease. Thus, changes in temperature of the continuously heated resistor are monitored while the cantilever is scanned over data bits, providing a means of detecting the bits. Erasing for subsequent rewriting is carried out by thermal reflow of the storage field by heating the medium to 150°C for a few seconds. The smoothness of the reflown medium allows multiple rewriting of the same storage field. Bit sizes ranging between 10 and 50 nm have been achieved by using a 32 × 32 (1,024) array write/read chip (3 mm × 3 mm). It has been reported that tip wear occurs by the contact between tip and Si substrate during writing. Tip wear is considered a major concern for the device reliability.

1.6 Role of Micro/Nanotribology and Micro/Nanomechanics in Magnetic Storage Devices and MEMS/NEMS

The magnetic storage devices and MEMS/NEMS are the two examples where micro/nanotribological and micro/nanomechanical tools and techniques are essential for studies of micro/nano scale phenomena. Magnetic storage components

continue to shrink in physical dimensions. Thicknesses of hard solid coating and liquid lubricant coatings on the magnetic disk surface continue to decrease. Number of contact recording devices are at various stages of development. Surface roughnesses of the storage components continue to decrease and are expected to approach to about 0.5 nm RMS or lower. Interface studies of components with ultra-thin coatings can be ideally performed using micro/nanotribological and micro/nanomechanical tools and techniques.

In the case of MEMS/NEMS, the friction and wear problems of ultrasmall moving components generally made of single-crystal silicon, polysilicon films or polymers need to be addressed for high performance, long life, and reliability. Molecularly-thin films of solid and/or liquids are used for low friction and wear in many applications. Again, interfacial phenomena in MEMS/NEMS can be ideally studied using micro/nanotribological and micro/nanomechanical tools and techniques.

1.7 Organization of the Book

The introductory book integrates knowledge of nanotribology and nanomechanics. The book starts with the definition of tribology, history of tribology and micro/nanotribology, its industrial significance, various measurement techniques employed, followed by various industrial applications. The remaining book is divided into four parts. The first part introduces scanning probe microscopy. The second part provides an overview of nanotechnology and nanomechanics. The third part provides an overview of molecularly-thick films for lubrication. And the last part focuses on nanotribology and nanomechanics studies conducted for various industrial applications.

References

1. P. Jost, *Lubrication (Tribology) – A Report on the Present Position and Industry's Needs*. (Department. of Education and Science, H.M. Stationary Office, 1966)
2. D. Dowson, *History of Tribology*, 2nd edn. (Institute of Mechanical Engineers, London, 1998)
3. C.S.C. Davidson, Bearings since the Stone Age. Engineering **183**, 2–5 (1957)
4. A.G. Layard, *Discoveries in the Ruins of Nineveh and Babylon, volume I, II* (Murray, London, 1853)
5. G. Amontons, De la resistance causee dans les machines. Mem. Acad. R. A. **1706**, 257–282 (1699)
6. C.A. Coulomb, Theorie des machines simples, en ayant regard an frottement de leurs parties et a la roideur des cordages. Mem. Math. Phys. X, Paris **10**, 161–342 (1785)
7. W.F. Parish, Three thousand years of progress in the development of machinery and lubricants for the hand crafts. Mill Factory **16**, 17 (1935)
8. B. Tower, Report on friction experiments. Proc. Inst. Mech. Eng. **632**, 29–35 (1884)
9. O.O. Reynolds, On the theory of lubrication and its applications to Mr. Beauchamp tower's experiments. Philos. Trans. R. Soc. Lond. **117**, 157–234 (1886)
10. N.P. Petroff, Friction in machines and the effects of the lubricant. Eng. J. 71–140, 228–279, 377–436, 535–564 (1883)

11. R. Holm, *Electrical Contacts* (Springer, Berlin, 1946)
12. F.P. Bowden, D. Tabor, *The Friction and Lubrication of Solids*, vols 1, 2. (Clarendon, Oxford, 1950, 1964)
13. B. Bhushan, *Tribology and Mechanics of Magnetic Storage Devices*, 2nd edn. (Springer, New York, 1996)
14. B. Bhushan, *Mechanics and Reliability of Flexible Magnetic Media*, 2nd edn. (Springer, New York, 2000)
15. B. Bhushan, *Introduction to Tribology* (Wiley, New York, 2002)
16. B. Bhushan, *Springer Handbook of Nanotechnology*, 1st edn. (Springer, Berlin, 2004)
17. B. Bhushan, B.K. Gupta, *Handbook of Tribology: Materials, Coatings, and Surface Treatments* (McGraw-Hill, New York, 1991)
18. P. Jost, *Economic Impact of Tribology*, vol 423 of NBS Spec. Pub. Proc. Mechanical Failures Prevention Group, 1976
19. B. Bhushan, J.N. Israelachvili, U. Landman, Nanotribology: Friction, wear and lubrication at the atomic scale. Nature **374**, 607–616 (1995)
20. B. Bhushan, *Micro/Nanotribology and its Applications*. NATO ASI Series E: Applied Sciences, vol. 330 (Kluwer, Dordrecht, 1997)
21. B. Bhushan, *Handbook of Micro/Nanotribology*, 2nd edn. (CRC, Boca Raton, 1999)
22. B. Bhushan, *Fundamentals of Tribology and Bridging the Gap Between the Macro- and Micro/Nanoscales*. NATO Science Series II: Mathematics, Physics, and Chemistry, vol. 10 (Kluwer, Dordrecht, 2001)
23. B. Bhushan, H. Fuchs, S. Hosaka, *Applied Scanning Probe Methods* (Springer, Berlin, 2004)
24. G. Binnig, H. Rohrer, Ch Gerber, E. Weibel, Surface studies by scanning tunnelling microscopy. Phys. Rev. Lett. **49**, 57–61 (1982)
25. G. Binnig, C.F. Quate, Ch Gerber, Atomic force microscope. Phys. Rev. Lett. **56**, 930–933 (1986)
26. G. Binnig, Ch Gerber, E. Stoll, T.R. Albrecht, C.F. Quate, Atomic resolution with atomic force microscope. Europhys. Lett. **3**, 1281–1286 (1987)
27. D. Tabor, R.H.S. Winterton, The direct measurement of normal and retarded van der Waals forces. Proc. R. Soc. Lond. A **312**, 435–450 (1969)
28. S. Alexander, L. Hellemans, O. Marti, J. Schneir, V. Elings, P.K. Hansma, An atomic-resolution atomic-force microscope implemented using an optical lever. J. Appl. Phys. **65**, 164–167 (1989)
29. B. Bhushan, J. Ruan, Atomic-scale friction measurements using friction force microscopy: Part II – application to magnetic media. ASME J. Tribol. **116**, 389–396 (1994)
30. J. Ruan, B. Bhushan, Atomic-scale friction measurements using friction force microscopy: Part I – general principles and new measurement techniques. ASME J. Tribol **116**, 378–388 (1994)
31. J. Ruan, B. Bhushan, Atomic-scale and microscale friction of graphite and diamond using friction force microscopy. J. Appl. Phys. **76**, 5022–5035 (1994)
32. G. Meyer, N.M. Amer, Novel optical approach to atomic force microscopy. Appl. Phys. Lett. **53**, 1045–1047 (1988)
33. B. Bhushan, V.N. Koinkar, J. Ruan, Microtribology of magnetic media. Proc. IME J J. Eng. Tribol **208**, 17–29 (1994)
34. J.N. Israelachvili, D. Tabor, The measurement of van der Waals dispersion forces in the range of 1.5 to 130 nm. Proc. Roy. Soc. Lond. A **331**, 19–38 (1972)
35. J.N. Israelachvili, G.E. Adams, Measurement of friction between two mica surfaces in aqueous electrolyte solutions in the range 0100 nm. J. Chem. Soc. Faraday Trans. I **74**, 975–1001 (1978)
36. J. Klein, Forces between mica surfaces bearing layers of adsorbed polystyrene in cyclohexane. Nature **288**, 248–250 (1980)
37. D.Y.C. Chan, R.G. Horn, The drainage of thin liquid films between solid surfaces. J. Chem. Phys. **83**, 5311–5324 (1985)

38. J.N. Israelachvili, P.M. McGuiggan, A.M. Homola, Dynamic properties of molecularly thin liquid films. Science **240**, 189–190 (1988)
39. J. Klein, D. Perahia, S. Warburg, Forces between polymer-bearing surfaces undergoing shear. Nature **352**, 143–145 (1991)
40. J. van Alsten, S. Granick, Molecular tribology of ultrathin liquid films. Phys. Rev. Lett. **61**, 2570–2573 (1988)
41. J. Peachey, J. van Alsten, S. Granick, Design of an apparatus to measure the shear response of ultrathin liquid films. Rev. Sci. Instrum. **62**, 463–473 (1991)
42. J.N. Israelachvili, Techniques for direct measurements of forces between surfaces in liquids at the atomic scale. Chemtracts. Anal. Phys. Chem **1**, 1–12 (1989)
43. G. Luengo, F.J. Schmitt, R. Hill, J.N. Israelachvili, Thin film bulk rheology and tribology of confined polymer melts: contrasts with build properties. Macromolecules **30**, 2482–2494 (1997)
44. J. van Alsten, S. Granick, Shear rheology in a confined geometry – polysiloxane melts. Macromolecules **23**, 4856–4862 (1990)
45. A.M. Homola, J.N. Israelachvili, M.L. Gee, P.M. McGuiggan, Measurement of and relation between the adhesion and friction of two surfaces separated by thin liquid and polymer films. ASME J. Tribol **111**, 675–682 (1989)
46. M.L. Gee, P.M. McGuiggan, J.N. Israelachvili, A.M. Homola, Liquid to solid-like transitions of molecularly thin films under shear. J. Chem. Phys. **93**, 1895–1906 (1990)
47. S. Granick, Motions and relaxations of confined liquids. Science **253**, 1374–1379 (1991)
48. A. Tonck, J.M. Georges, J.L. Loubet, Measurements of intermolecular forces and the rheology of dodecane between alumina surfaces. J. Colloid Interface Sci. **126**, 1540–1563 (1988)
49. J.M. Georges, S. Millot, J.L. Loubet, A. Tonck, Drainage of thin liquid films between relatively smooth surfaces. J. Chem. Phys. **98**, 7345–7360 (1993)
50. J.M. Georges, A. Tonck, D. Mazuyer, Interfacial friction of wetted monolayers. Wear **175**, 59–62 (1994)
51. J.N. Israelachvili, *Intermolecular and Surface Forces*, 2nd edn. (Academic, London, 1992)
52. R.G. Horn, Surface forces and their action in ceramic materials. J. Am. Ceram. Soc. **73**, 1117–1135 (1990)
53. A.M. Homola, *Interfacial Friction of Molecularly Thin Liquid Films* (World Scientific, Singapore, 1993), pp. 271–298
54. A.M. Homola, J.N. Israelachvili, P.M. McGuiggan, M.L. Gee, Fundamental experimental studies in tribology: the transition from interfacial friction of undamaged molecularly smooth surfaces. Wear **136**, 65–83 (1990)
55. R.M. Pashley, Hydration forces between solid surfaces in aqueous electrolyte solutions. J. Colloid Interface Sci. **80**, 153–162 (1981)
56. R.G. Horn, D.T. Smith, W. Haller, Surface forces and viscosity of water measured between silica sheets. Chem. Phys. Lett. **162**, 404–408 (1989)
57. R.G. Horn, J.N. Israelachvili, Molecular organization and viscosity of a thin film of molten polymer between two surfaces as probed by force measurements. Macromolecules **21**, 2836–2841 (1988)
58. H.K. Christenson, Adhesion between surfaces in unsaturated vapors – a reexamination of the influence of meniscus curvature and surface forces. J. Colloid Interface Sci. **121**, 170–178 (1988)
59. C.P. Smith, M. Maeda, L. Atanasoska, H.S. White, Ultrathin platinum films on mica and measurement of forces at the platinum/water interface. J. Phys. Chem. **95**, 199–205 (1988)
60. S.J. Hirz, A.M. Homola, G. Hadzioannou, S.W. Frank, Effect of substrate on shearing properties of ultrathin polymer films. Langmuir **8**, 328–333 (1992)
61. S.S. Patel, M. Tirrell, Measurement of forces between surfaces in polymer fluids. Annu. Rev. Phys. Chem. **40**, 597–635 (1989)
62. J.N. Israelachvili, Solvation forces and liquid structure – as probed by direct force measurements. Acc. Chem. Res. **20**, 415–421 (1987)

63. J.N. Israelachvili, P.M. McGuiggan, Forces between surface in liquids. Science **241**, 795–800 (1988)
64. A.M. Homola, Measurement of and relation between the adhesion and friction of two surfaces separated by thin liquid and polymer films. ASME J. Tribol. **111**, 675–682 (1989)
65. A.M. Homola, H.V. Nguyen, G. Hadzioannou, Influence of monomer architecture on the shear properties of molecularly thin polymer melts. J. Chem. Phys. **94**, 2346–2351 (1991)
66. J. van Alsten, S. Granick, Tribology studied using atomically smooth surfaces. Tribol. Trans. **33**, 436–446 (1990)
67. W.W. Hu, G.A. Carson, S. Granick, Relaxation time of confined liquids under shear. Phys. Rev. Lett. **66**, 2758–2761 (1991)
68. J.L. Loubet, M. Bauer, A. Tonck, S. Bec, B. Gauthier-Manuel, *Nanoindentation with a Surface Force Apparatus* (Kluwer, Dordrecht, 1993), pp. 429–447
69. B. Bhushan, *Macro- and microtribology of magnetic storage devices*, vol. 2 (CRC, Boca Raton, 2001), pp. 1413–1513
70. B. Bhushan, *Tribology Issues and Opportunities in MEMS* (Kluwer, Dordrecht, 1998)
71. L.J. Hornbeck, W.E. Nelson, *Bistable Deformable Mirror Devices*, *OSA Technical Digest Series*, vol. 8. (OSA, Washington, DC, 1988), pp. 107–110
72. L.J. Hornbeck, A digital light processing™ update – status and future applications. Proc. SPIE **3634**, 158–170 (1999)
73. P. Vettinger, J. Brugger, M. Despont, U. Dreschier, U. Duerig, W. Haeberie, Ultrahigh density, high data-rate NEMS based AFM data storage systems. Microelectron. Eng. **46**, 11–27 (1999)